

1  
2 **Simultaneous Prediction of Morphologies of a**  
3 **Critical Nucleus and an Equilibrium Precipitate**  
4 **in Solids**

5 Lei Zhang<sup>1</sup>, Long-Qing Chen<sup>2</sup> and Qiang Du<sup>1,2,\*</sup>

6 <sup>1</sup> Department of Mathematics, Penn State University, PA 16802, USA.

7 <sup>2</sup> Department of Materials Science and Engineering, Penn State University, PA 16802,  
8 USA.

9 Received xxx 200x; Accepted (in revised version) xxx 200x

10 Communicated by Jie Shen

11 Available online xxx

12  

---

**Abstract.** We investigate the critical nucleus and equilibrium morphologies during precipitation of a second-phase particle in a solid. We show that a combination of diffuse-interface description and a constrained string method is able to predict both the critical nucleus and equilibrium precipitate morphologies simultaneously without *a priori* assumptions. Using the cubic to cubic transformation as an example, it is demonstrated that the maximum composition within a critical nucleus can be either higher or lower than that of equilibrium precipitate while the morphology of an equilibrium precipitate may exhibit lower symmetry than the critical nucleus resulted from elastic interactions.

13 **AMS subject classifications:** (or PACS) To be provided by authors.

14 **Key words:** Phase field, diffuse interface, nucleation, critical nucleus, constrained string method,  
15 elasticity.

16  

---

**1 Introduction**

17  
18 Precipitation is a common, natural process which takes place in a supersaturated solid  
19 or liquid solution, e.g., during isothermal annealing of a quenched homogeneous al-  
20 loy within a two-phase field of a phase diagram. It is the basic process that underlies  
21 the development of many advanced materials such as high-temperature superalloys and  
22 ultralight aluminum and magnesium alloys. The precipitate microstructure (the num-  
23 ber density, volume fraction, and morphology) is the dominant factor that determines

\*Corresponding author. Email addresses: zhang\_1@math.psu.edu (L. Zhang), lqc3@psu.edu (L.-Q. Chen), qdu@math.psu.edu (Q. Du)

24 the mechanical properties of a solid. One of the main challenges in predicting precipi-  
25 tate microstructures in solids has been the determination of precipitate particle morphol-  
26 ogy because of the presence of both interfacial energy anisotropy and anisotropic elastic  
27 interactions. As the majority of precipitation reactions in solids take place through a  
28 nucleation-and-growth mechanism followed by particle coarsening, there are two ther-  
29 modynamically well-defined morphologies: the morphology of a critical nucleus and the  
30 equilibrium morphology of a precipitate particle.

31 In classical nucleation models, a critical nucleus is usually assumed to be spherical  
32 and critical radius is determined by a competition between a bulk free energy decrease  
33 which is proportional to volume and an interfacial energy increase which is proportional  
34 to interfacial area. In a diffuse-interface description, a critical nucleus is defined as the  
35 composition or order parameter fluctuation having the minimum free energy increase  
36 among all fluctuations which lead to nucleation, i.e., the saddle point configuration along  
37 the minimum energy path (MEP) between the metastable initial phase represented by a  
38 local minimum in the free energy landscape and the equilibrium phase represented by  
39 the global minimum. Therefore, nucleation of new precipitate particles requires over-  
40 coming a thermodynamic barrier. The magnitude of the nucleation barrier, and thus the  
41 nucleation rate, or the resulted precipitate particle density, is strongly dependent on the  
42 morphology of critical nuclei. On the other hand, following nucleation and growth, the  
43 morphology and volume fraction of precipitate particles during coarsening are generally  
44 close to equilibrium. The particle morphology and volume fraction during coarsening  
45 together with the particle density predicted from nucleation provide all the information  
46 that is needed for predicting the strength of a solid in mechanistic models.

47 There have been extensive studies, particularly numerical simulations, of equilib-  
48 rium shapes of a precipitate particle in solids using both sharp- and diffuse-interface  
49 approaches [5, 7, 8, 11–13]. Attempts have also been made to predict the morphology  
50 of a critical nucleus in solids by taking into account both interfacial energy anisotropy  
51 and anisotropic elastic interactions [9, 10, 14–16]. For example, we showed that one can  
52 predict the morphology of a critical nucleus in a system going through a phase transi-  
53 tion [14–16] using a combination of the diffuse-interface (phase-field) description and the  
54 minimax algorithm based on the mountain pass theorem. The main objective of this let-  
55 ter is to report a first attempt to predict the morphology of a critical nucleus as well as  
56 the equilibrium morphology of a precipitate simultaneously within the same physical  
57 model and mathematical formulation. A concentration field that conserves the average  
58 concentration is considered as an illustration. We extend the string method [3, 4] to sys-  
59 tems with constraints through a novel augmented Lagrange multiplier formulation. This  
60 leads to an effective constrained string method which may be useful in the study of many  
61 constrained barrier crossing problems in physics, chemistry and biology. In this work,  
62 we demonstrate that a combination of diffuse-interface description and the constrained  
63 string method can simultaneously predict the morphologies of a critical nucleus and an  
64 equilibrium precipitate which can be dramatically different.

## 2 Diffuse interface model

Following the diffuse-interface theory of Cahn-Hilliard [1], we consider a conserved field  $c$  which describes the concentration distribution in a binary solid. The change of the total free energy,  $F_t$ , arising from the compositional fluctuation in an initially homogeneous state with  $c_0$  is given by

$$F_t(c) = \int_{\Omega} \left( \frac{1}{2} |A \nabla c|^2 + \delta f(c) \right) dx + \beta E_e(c). \quad (2.1)$$

We use the domain  $\Omega = (-1, 1)^d$  with  $d$  being the space dimension. A periodic boundary condition is used for  $c$  with the period sufficiently large in comparison with the size of the nucleus and the equilibrium particle so the effect of boundary conditions is negligible. The gradient energy coefficient  $A$  is a constant diagonal tensor for isotropic interfacial energy, while for anisotropic interfacial energy, it can be made to be either directionally dependent or dependent on the derivatives of  $c$ . In [14], the effect of anisotropic interfacial energy on the critical nuclei morphology has been examined in the case of a non-conserved field. In this work, we choose to focus on the case of isotropic interfacial energy with  $A$  being a constant multiple of the identity tensor. The local free energy density change  $\delta f(c)$ , arising from a compositional fluctuation around the homogeneous state with composition  $c_0$ , is given by

$$\delta f(c) = \frac{1}{4\kappa} [(c^2 - 1)^2 - (c_0^2 - 1)^2 - 4(c - c_0)(c_0^3 - c_0)],$$

where  $\kappa$  is a coefficient of energy density. The plots of  $\delta f = \delta f(c)$  are given in Fig. 1 for different  $c_0$  at  $\kappa = 0.03$ , with  $c_s = -\sqrt{3}/3$  being the spinodal composition.

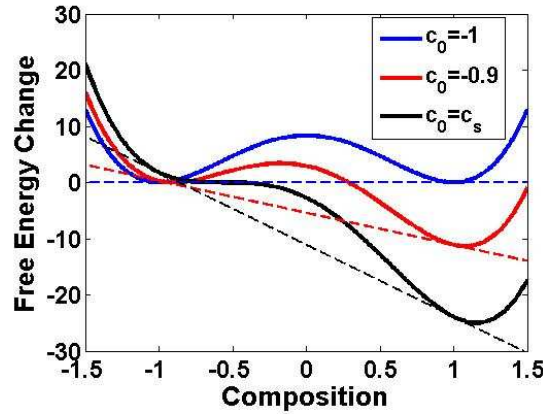


Figure 1: Free energy change for  $c_0 = -1, -0.9$  and  $c_s$ .

Assuming that the elastic modulus is anisotropic but homogeneous, the microscopic elasticity theory of Khachatryan [6] can be conveniently employed to efficiently calculate the elastic strain energy for simply connected coherent inclusions in a solid. For the

75 case of cubic precipitates in a cubic matrix, the elastic energy contribution can be written  
76 as

$$E_e(c) = \frac{1}{2(2\pi)^d} \int_{\hat{\Omega}} d\mathbf{k} B(\mathbf{n}) |\hat{c}(\mathbf{k}) - \hat{c}_0(\mathbf{k})|^2. \quad (2.2)$$

77  $\hat{c}(\mathbf{k})$  is the Fourier transform of  $c(\mathbf{x})$ . The integration in (2.2) is over the reciprocal space  
78  $\hat{\Omega}$  of the reciprocal lattice vector  $\mathbf{k}$ ,  $\mathbf{n} = \mathbf{k}/|\mathbf{k}| = (n_1, n_2, n_3)$  is the normalized unit vector and  
79  $B(\mathbf{n})$  is given by [6]

$$B(\mathbf{n}) = 3(c_{11} + 2c_{12})\epsilon_0^2 - \frac{(c_{11} + 2c_{12})^2\epsilon_0^2(1 + 2\zeta s(\mathbf{n}) + 3\zeta^2 n_1^2 n_2^2 n_3^2)}{c_{11} + \zeta(c_{11} + c_{12})s(\mathbf{n}) + \zeta^2(c_{11} + 2c_{12} + c_{44})n_1^2 n_2^2 n_3^2}, \quad (2.3)$$

80 where  $\zeta = (c_{11} - c_{12} - 2c_{44})/c_{44}$  is the elastic anisotropic factor with  $c_{11}, c_{12}, c_{44}$  being elastic  
81 constants in the Voigt's notation,  $\epsilon_0$  is the lattice mismatch between the new nucleating  
82 cubic phase and the parent cubic phase, and  $s(\mathbf{n}) = n_1^2 n_2^2 + n_1^2 n_3^2 + n_2^2 n_3^2$ . We set, in particular  
83 that,  $\mathbf{n} = 0$  if  $\mathbf{k} = 0$ .

84 Rather than varying the magnitude of lattice mismatch and elastic constants, a fac-  
85 tor  $\beta$  is introduced in (2.1) to study the effect of relative elastic energy contribution to  
86 chemical driving force on the critical nucleus morphology and equilibrium particle mor-  
87 phology.

88 For a conserved field with profile  $c=c(x)$ , the computation of saddle points and the  
89 minimum energy path for the energy functional (2.1) subject to the constraint

$$\int_{\Omega} (c(x) - c_0) dx = 0. \quad (2.4)$$

90 is carried out via the constrained string method which is a natural extension of the simpli-  
91 fied string method originally developed by E, Ren and Vanden-Eijnden [3,4]. We outline  
92 the algorithmic procedures here. Some related mathematical theory can be found in [2]  
93 while detailed numerical analysis will be given elsewhere.

The string methods proceed by evolving a string, i.e., a smooth curve with intrinsic parametrization, to the MEP between two metastable/stable regions in configuration space. Specifically, let  $\varphi(\alpha, t)$  denote the instantaneous position (representing the composition profile in our case) of the string with  $\alpha$  being a suitable parametrization. For an energy  $E=E(\varphi)$ , the evolution of the string is based on first taking a gradient decent direction via the dynamic equation

$$\varphi_t = -\frac{\delta E}{\delta \varphi}(\varphi),$$

94 then followed by a projection step that maps  $\varphi$  back to a configuration satisfying the  
95 specified parametrization [4]. Here,  $\frac{\delta E}{\delta \varphi}$  represents the variational derivative of the en-  
96 ergy  $E$  with respect to  $\varphi$ . In practice, a commonly used parametrization for a string  
97 discretized by a finite number of line segments is to enforce an equal segment length con-  
98 dition through an interpolation procedure [4]. Sufficient number of segments are needed

99 to ensure both the convergence and the accuracy of the algorithm. Based on such an  
 100 idea, we developed a constrained string method to find the MEP on general constrained  
 101 manifolds. It follows essentially the string method with additional treatment of the con-  
 102 straints.

The constrained string method allows several equivalent formulations such as the penalty or Lagrange multiplier methods. Yet, some formulations are more natural and robust than others and require less parameter tuning. One particularly effective approach is based on the augmented Lagrange multiplier method. Its application to the energy (2.1), subject to the simple constraint (2.4), amounts to consider a modified total energy involving two parameters  $\lambda$  and  $M$ :

$$E_{\lambda}(\varphi) = F_t(\varphi) + \lambda \int_{\Omega} (\varphi - c_0) dx + M \left( \int_{\Omega} (\varphi - c_0) dx \right)^2.$$

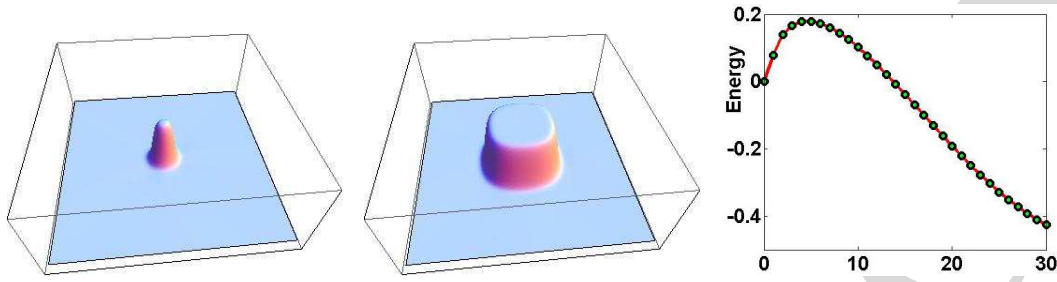
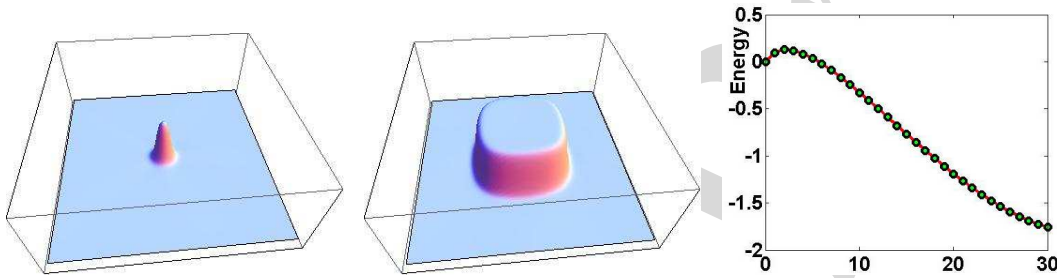
For a fixed positive penalty constant  $M$ , we solve for the constrained string, via the following iterations: first, given  $\lambda_j$ , we apply the string method [4] to the modified energy  $E_{\lambda_j} = E_{\lambda_j}(\varphi)$  to solve for  $\varphi_j$ ; then, with  $\varphi_j$  known, we update  $\lambda_j$  by  $\lambda_{j+1}$  via:

$$\lambda_{j+1} = \lambda_j + 2M \int_{\Omega} (\varphi_j - c_0) dx.$$

103 We iterate between these two steps until convergence. At the end of iteration, the con-  
 104 strained MEP is found with the equation (2.4) satisfied along the string, and the limit of  $\lambda_j$   
 105 gives the corresponding Lagrange multiplier. Adopting this formulation, the implemen-  
 106 tation of the constrained string method is straightforward and it assures the satisfaction  
 107 of the constraint without requiring  $M$  to be exceedingly large, thus reducing the stiffness  
 108 of the dynamic system. The constrained string method including the augmented La-  
 109 grange multiplier formulation can be derived for very general energies and constrained  
 110 manifolds and thus have many potential applications. For the case of the energy func-  
 111 tional  $F_t$ , each point of the string corresponds to a composition profile along the MEP.  
 112 The critical nucleus is determined by the composition profile  $c=c(x)$  which is recovered  
 113 from the saddle point corresponding to the point on the converged MEP with the highest  
 114 energy.

### 115 3 Numerical simulations

116 The model and algorithm described above allows us to determine both the critical nu-  
 117 cleus and equilibrium precipitate. As an illustration, we focus on the two-dimensional  
 118 example of a cubic to cubic transformation. We fix one end of the string to be the initial  
 119 state representing a uniform composition with  $c(x) = c_0$  in  $\Omega$ , while allowing the other  
 120 end to move but generally within the energy well of the ground state or equilibrium solu-  
 121 tion. We use 31 points (30 line segments) to discretize the string and the Fourier spectral  
 122 method with a  $256 \times 256$  grid for computing each composition profile, i.e., point on the

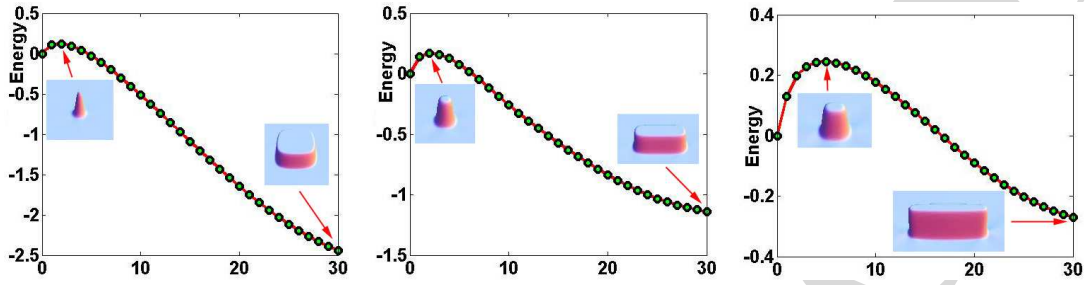
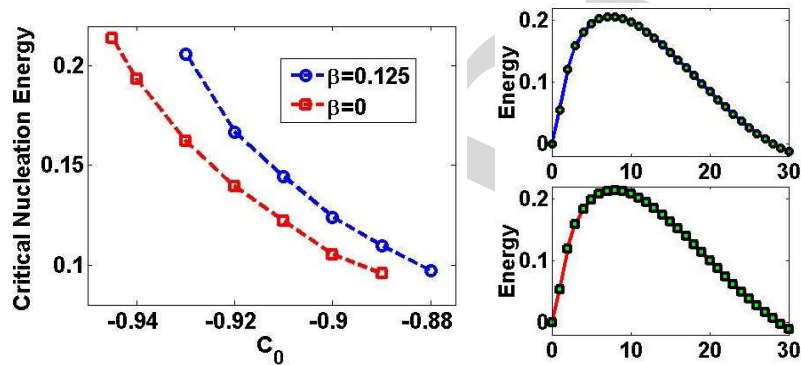
Figure 2: Critical nucleus, equilibrium and MEP for  $c_0 = -0.9$ .Figure 3: Critical nucleus, equilibrium and MEP for  $c_0 = -0.88$ .

123 string. An adaptive rescaling of the computational domain along the string can be used to  
 124 further improve the resolution. Numerical tests were conducted to ensure that sufficient  
 125 resolution can be achieved. We fix the parameters  $A_1 = A_2 = 1.56 \times 10^{-4}$ ,  $c_{11} = 250$ ,  $c_{12} = 150$ ,  
 126  $c_{44} = 200$  and  $\epsilon_0 = 0.02$ . Since both critical nucleus and equilibrium solution are relatively  
 127 small in comparison to the spatial domain  $\Omega$ , their plots are magnified by a factor of 2 in  
 128 order to get a better view.

129 In Fig. 2, for  $\kappa = 0.7$  and  $\beta = 0.5$ , we plot the critical nucleus (left) and equilibrium so-  
 130 lution (center) and the MEP (right) in the presence of the long-range elastic interactions  
 131 corresponding to an average composition  $c_0 = -0.9$ . One of the interesting observations is  
 132 that the maximum composition within the critical nucleus is about 5% higher than that  
 133 of the equilibrium precipitate. For this  $c_0$ , however, both the critical nucleus and equilib-  
 134 rium precipitate have the same cubic symmetry due to the elastic energy interactions.

135 Another example is shown in Fig. 3 when  $c_0$  is changed to  $-0.88$ . As  $c_0$  is close to the  
 136 spinodal point, the interface of critical nucleus becomes more diffusive. The composition  
 137 value at the center of a critical nucleus decreases and is about 5% smaller than the com-  
 138 position of the equilibrium precipitate. Moreover, the size of the equilibrium precipitate  
 139 is larger for  $c_0 = -0.88$  than for  $c_0 = -0.9$  as a result of higher supersaturation.

140 In both Figs. 2 and 3, the MEP plots reveal how the energy values change from the  
 141 initial state to the final equilibrium state along points on the string (corresponding to total  
 142 31 different composition profiles). The value of critical energy needed to nucleate a new  
 143 particle for  $c_0 = -0.88$  is 0.1282 which is significantly lower than the value of 0.1792 for  
 144  $c_0 = -0.9$ .

Figure 4: Calculated MEPs for  $\beta=0.5, 1$  and  $1.5$  with inserts showing the critical nuclei and equilibria.Figure 5: Critical nucleation energy with changing  $c_0$  for  $\beta=0.125$  and  $0$  (left) and MEPs (right) for  $c_0=-0.93, \beta=0.125$  and  $c_0=-0.945, \beta=0$ .

145 To examine the effect of elastic energy contributions, we fix the chemical driving force  
 146 with  $c_0 = -0.85$  and  $\kappa = 1$ , and increase  $\beta$  to compute the MEPs. In Fig. 4 (left), we plot the  
 147 MEPs (with the compositional profiles for the critical nucleus and equilibrium precipitate  
 148 as inserts) for different values of  $\beta$ . At a relatively small elastic energy contribution,  
 149 both the critical nucleus and the equilibrium precipitate display a cubic symmetry. With  
 150 higher elastic strain energy contribution, while the critical nucleus maintains the cubic  
 151 symmetry, the equilibrium precipitate is plate-like with only two-fold symmetry (Fig. 4,  
 152 center). As we further increase the elastic energy contribution, for example,  $\beta = 1.5$ , both  
 153 the critical nucleus and the equilibrium precipitate exhibit plate-shaped particles (Fig. 4,  
 154 right). We also observe the increases in both the critical nucleus size (see the inserts) and  
 155 the nucleation energy barrier (from 0.1222 to 0.1708 and 0.2449) with increasing elastic  
 156 energy contributions.

157 The influence of elastic energy contributions on the morphologies of both critical nu-  
 158 clei and equilibrium precipitates can be understood from the competition between in-  
 159 terfacial energy and elastic strain energy. The total interfacial energy is proportional to  
 160 interfacial area between a particle and the matrix while the total elastic strain energy is  
 161 proportional to the volume of the particle. Since the size of a critical nucleus is signifi-  
 162 cantly smaller than that of an equilibrium precipitate, it is expected that the elastic energy

will have a lesser influence on the critical nucleus (assuming the interfacial coherency between the particle and matrix is always maintained during the entire evolution process). Minimization of elastic strain energy leads to plate-shaped particles while minimization of interfacial energy (assuming isotropic) leads to spherical shapes. Therefore, as the elastic strain energy contribution increases, the shape of the equilibrium precipitate bifurcates first from being cubic to plate-shaped before the critical nucleus does.

To further understand the elastic energy contributions, in Fig. 5 (left), the critical free energy of formation as a function of average composition  $c_0$  is plotted for the case without the elasticity contribution  $\beta=0$  (red squares), and for critical nuclei with  $\beta=0.125$  (blue circles). We take  $\kappa=1$  in both cases. As expected, with the increase of the average composition, the size of critical nuclei (with cubic symmetry) is reduced and the critical nucleation energy decreases. This dependence is similar to that predicted from the classical nucleation theory for spherical particles. We also notice that, for the given parameters and elastic energy, the smallest  $c_0$  which allows nucleation to happen is  $-0.93$ , where the energy of equilibrium solution is very close to the initial-state energy (Fig. 5, top right). If  $c_0$  is smaller than  $-0.93$ , the energy of an equilibrium precipitate becomes higher than the initial homogeneous state, indicating that the initial uniform state could be globally stable so that the elastic energy contribution can prevent the nucleation process from occurring, i.e. coherency strain energy contribution shifts the equilibrium phase boundary. Without elasticity, nucleation can still take place with an even smaller  $c_0=-0.945$  (Fig. 5, bottom right).

## 4 Summary

In summary, we report a new approach for computing the morphologies of both critical nuclei and equilibrium precipitates without *a priori* shape assumptions. Our calculations reveal that the morphology of a critical nucleus can be dramatically different from the equilibrium one due to the elastic energy contributions. We plan to extend the approach to treat systems with defects such as dislocations and interfaces, i.e., processes of heterogeneous nucleation. Moreover, while the focus of this letter is on the precipitate nucleation and the equilibrium state, the mathematical and computational framework can be potentially applied to other constrained barrier crossing problems in physics, chemistry and biology, including examples like the saddle point search for activated states in solid state diffusion using density function theory, and the determination of domain morphology of a critical nucleus and a switched state in ferroelectric solids under an applied electric field.

## Acknowledgments

This research is supported in part by NSF-DMS 0712744, NSF DMR-0710483 and NSF-IIP 541674 Center for Computational Materials Design (CCMD).

200 **References**

- 201 [1] J. Cahn and J. Hilliard, Free energy of a nonuniform system. III. Nucleation in a two-  
202 component incompressible fluid, *J. Chem. Phys.*, 31 (1959), pp.688-699.
- 203 [2] Q. Du and L. Zhang, A constrained string method and its numerical analysis, to appear in  
204 *Comm. Math. Sci.*, 2009.
- 205 [3] W. E, W. Ren and E Vanden-Eijnden, String method for the study of rare events, *Phys. Rev.*  
206 *B*, 66, 052301, (2002).
- 207 [4] W. E, W. Ren and E Vanden-Eijnden, Simplified and improved string method for computing  
208 the minimum energy paths in barrier-crossing events, *J. Chem. Phys.*, 126, 164103, 2007.
- 209 [5] H.J. Jou, P.H. Leo and J.S. Lowengrub, Microstructural Evolution in Inhomogeneous Elastic  
210 Media, *J. Comp. Phys.*, 131 (1997), pp.109-148.
- 211 [6] A.G. Khachaturyan, *Theory of Structural Transformations in Solids*, Wiley, New York,  
212 (1983).
- 213 [7] J.K. Lee, Morphology of coherent precipitates via a discrete atom method, *Mat. Sci. Eng. A*,  
214 238 (1997), pp.1-12.
- 215 [8] R. Mueller and D. Gross, 3D simulation of equilibrium morphologies of precipitates, *Comp.*  
216 *Mat. Sci.*, 11 (1998), pp.35-44.
- 217 [9] A. Roy, J.M. Rickman, J.D. Gunton and K.R. Elder, Simulation study of nucleation in a phase-  
218 field model with nonlocal interactions, *Phys. Rev. E*, 57 (1998), pp.2610-2617.
- 219 [10] C. Shen, J.P. Simmons and Y. Wang, Effect of elastic interaction on nucleation: I. Calculation  
220 of the strain energy of nucleus formation in an elastically anisotropic crystal of arbitrary  
221 microstructure, *Acta Materialia*, 54 (2006), pp.5617-5630.
- 222 [11] M.E. Thompson and P.W. Voorhees, Equilibrium particle morphologies in elastically stressed  
223 coherent solids, *Acta Materialia*, 47 (1999), pp.983-996.
- 224 [12] Y. Wang, L.Q. Chen and A.G. Khachaturyan, Kinetics of strain-induced morphological trans-  
225 formation in cubic alloys with a miscibility gap, *Acta Materialia*, 41 (1993), pp.279-296.
- 226 [13] C. Wolverton, First-principles prediction of equilibrium precipitate shapes in Al-Cu alloys,  
227 *Phil. Mag. Lett.*, 79 (1999), pp.683-690.
- 228 [14] L. Zhang, L.Q. Chen and Q. Du, Morphology of critical nuclei in solid state phase transfor-  
229 mations, *Phys. Rev. Lett.*, 98, 265703 (2007)
- 230 [15] L. Zhang, L.Q. Chen and Q. Du, Diffuse-interface description of strain-dominated morphol-  
231 ogy of critical nuclei in phase transformations, *Acta Materialia*, 56 (2008), pp.3568-3576.
- 232 [16] L. Zhang, L.Q. Chen and Q. Du, Mathematical and Numerical Aspects of Phase-field Ap-  
233 proach to Critical Morphology in Solids, *J. Sci. Comput.*, 37 (2008), pp.89-102.